Proceedings of ICMMGH 2026 Symposium: Biomedical Imaging and AI Applications in Neurorehabilitation
DOI: 10.54254/2753-8818/2026.AU29754

Polymer Nanomedicine Size Calculation for Bone Cancer Application

Junqing Li

School of Materials Science and Engineering, Kunming University of Science and Technology, Kunming, China
784672223@qq.com

Abstract. Bone cancer has multiple treatment options, among which nanoparticle-based therapy offers significant advantages due to its low toxicity. To ensure therapeutic efficacy, nanoparticle size requires optimization. In this study, the Higuchi model was used to simulate the release rates of nanodrugs with different sizes in the bone microenvironment. The maximum nanoparticle size is constrained by the size of the bone tubule network in the bone microenvironment, while the minimum size considers the risk of rapid clearance of small nanoparticles via bone marrow sinuses. It was found that nanoparticles with a size range of 80–120 nm are suitable for the bone microenvironment, and the size dependence of nanoparticles in bone-targeted delivery was revealed. This study provides a theoretical basis for determining the appropriate size of spherical polymeric nanoparticles in the bone microenvironment and establishes a computable design paradigm for nanotherapies targeting diseases such as bone metastases.

Keywords: Higuchi model, Osteosarcoma, Polymeric Nanodrugs

1. Introduction

Bone cancer (e.g., osteosarcoma, bone metastasis) is a type of malignancy that severely impairs human health and quality of life. From the perspective of pathogenesis, bone cancer is classified into primary bone cancer and secondary bone cancer. Primary bone cancer typically occurs in the long bones of the limbs, while secondary bone cancer primarily affects the pelvis, spine, and other regions. For bone cancer treatment, traditional approaches usually include chemotherapy and surgical intervention. Surgical intervention is indicated when the cancer has not spread, whereas chemotherapy is suitable for treating undifferentiated reticulosarcoma (primary reticulum-cell sarcoma of bone), multiple myeloma, and certain bone metastases [1,2]. With the development of science and technology, drug therapy— which is less harmful to the human body—has garnered increasing attention and clinical application. Particularly, nanodrugs—a novel class of therapeutic agents—provide a more effective treatment strategy for cancer.

Nanoparticles are man-made microparticles. Nanoparticles commonly used in medicine typically refer to particles with sizes ranging from 1 to 100 nm [3]. However, submicron particles are also frequently referred to as "nanoparticles" in pharmaceutical and medical fields and are categorized into polymeric nanocrystals, liposomes, and solid lipid nanoparticles (SLNs) based on their

© 2025 The Authors. This is an open access article distributed under the terms of the Creative Commons Attribution License 4.0 (https://creativecommons.org/licenses/by/4.0/).

DOI: 10.54254/2753-8818/2026.AU29754

composition, function, and morphology [4]. Their forms may include latex, polymers, ceramic particles, metal particles, and carbon particles. Currently, nanoparticles are widely applied in medicine. Drugs loaded into nanoparticles have been shown to exhibit enhanced targeting ability, biocompatibility, and stability.

Nanomedicine has demonstrated great potential in the treatment of bone-related diseases, and its efficacy is highly dependent on the dynamic interactions between nanoparticles and the complex bone microenvironment. Beginning with the design requirements of nanomedicine, this study sequentially analyzes the effects of each requirement and ultimately explores the appropriate size of nanomedicines in the bone microenvironment using the Higuchi model. Bone tissue possesses a unique mineralized matrix structure, a multi-scale pore network (1–100 μm), and a dynamic mechanical stress microenvironment [5]. Integrating these environmental constraints, this study developed a nanomedicine release rate model for the bone microenvironment, which is highly valuable for predicting the efficacy of spherical polymeric nanomedicines in treating diseases such as bone metastatic cancer.

2. Problems in the treatment of bone cancer

Nanomedicines exhibit remarkable therapeutic potential for disease treatment due to their unique physicochemical properties, including high specific surface area, tunable surface chemistry, and enhanced penetration-retention (EPR) effect. However, a fundamental challenge lies in their inherent instability. During synthesis, storage, circulation, and delivery, key parameters of nanoparticles—including particle size, morphology, surface charge, and chemical composition—are highly prone to variation [6]. This variability primarily arises from spontaneous inter-particle aggregation and dynamic interactions with proteins, cells, and biomolecules in complex biological environments. Such instability directly results in deviations from their designed biological behaviors, leading to problems such as premature drug leakage, reduced targeting efficiency, and elevated off-target toxicity. For example, in the absence of targeting capabilities, zoledronic acid can induce symptoms such as osteonecrosis of the jaw (ONJ), renal failure, and hypocalcemia [7]. These challenges severely hinder the clinical translation and practical application of nanomedicines.

Among these parameters, size is one of the most critical physical factors that determine the blood circulation time, tissue penetration depth, cellular uptake mechanisms, and clearance pathways of nanomedicines. Thus, precise size design is crucial for optimizing their pharmacokinetics and pharmacodynamics. However, the complexity of size design presents another major challenge. First, research indicates that the size of nanomedicines significantly influences there in vivo distribution: larger particles (>200 nm) primarily accumulate in the liver and spleen and are cleared from the bloodstream by macrophages of the reticuloendothelial system. Smaller nanoparticles, by contrast, are restricted to tissue extravasation and renal clearance [8]. Furthermore, the nanomedicine-based treatment strategy for bone cancer outlined in this study must not only circulate effectively in the human body but also adapt to the complex bone microenvironment. The complexity of such design and preparation, coupled with the impact of the in vivo environment on size stability, constitutes a major barrier to the rational design of safe and effective nanomedicines.

DOI: 10.54254/2753-8818/2026.AU29754

3. Analysis of size, structure, and shape of nanomedicines

3.1. Effect of nanodrug size on therapeutic efficacy

Currently, various strategies and development approaches have been established for nanomedicines fabricated by encapsulating drugs within nanomaterials. This study focuses on polymeric nanomedicines. Aliphatic polyesters are among the most widely used polymers for fabricating polymeric nanoparticles due to their excellent biodegradability and biocompatibility. Among these, polylactic acid (PLA), polyglycolic acid (PGA), polycaprolactone (ε-caprolactone, PCL), and poly(lactide-co-glycolide) (PLGA) are the most frequently employed. To date, polymeric nanoparticles have been engineered into various forms, including polymer capsules, polymer micelles, polymeric nanospheres, dendrimers, and nanogels [9].

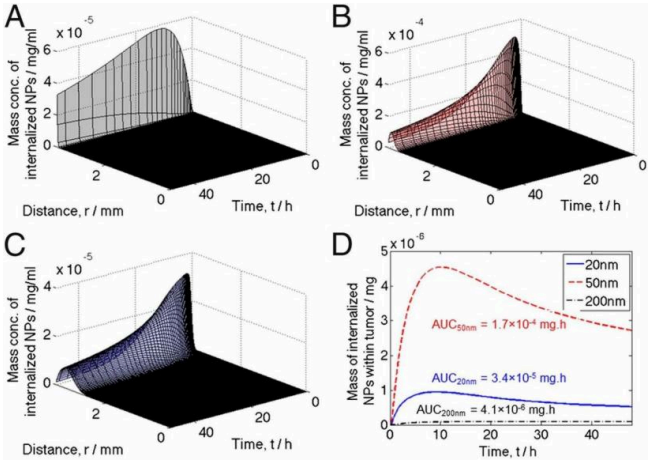


Figure 1. A mathematical model elucidating the spatiotemporal distribution of nanoparticles (NPs) within tumors. (A–C) illustrate the predicted concentration fields of internalized NP mass in a spherically symmetric tumor, plotted against radial distance from the tumor center (r) and time (t), for NPs with diameters of (A) 200 nm, (B) 50 nm, and (C) 20 nm. (D) displays the modeled temporal evolution of internalized NP mass for these three sizes over 48 hours. The vertical axis represents the total mass of internalized NPs within the spherical tumor (radius R = 3.5 mm)

The efficacy of nanomedicines is strongly influenced by their size. To investigate the size-dependent accumulation and retention of NPs in tumors. As shown in figure 1, Li Tang et al. established a mathematical framework describing the spatiotemporal distribution of NPs in a spherically symmetric tumor system [10]. Their model simulated key processes including NP diffusion into and out of the tumor, binding and dissociation from cell surfaces, and cellular internalization and exocytosis. Parameters were calibrated using experimental data from silica nanoconjugates (NCs) of 200 nm, 50 nm, and 20 nm diameters, with a best-fit linear regression model applied to estimate NP size-related parameters. The resulting spatiotemporal concentration profiles emerge from the interplay between NP transport dynamics (diffusion) and cellular uptake mechanisms. NP penetration depth into tumor spheroids is highly dependent on size: larger NPs diffuse more slowly, leading to more superficial distribution. The temporal evolution of the concentration profile is governed by the decay kinetics of NPs in the bulk phase, modulated by their transport, surface binding, and internalization into cancer cells [11]. The results demonstrate that, compared to 20 nm and 200 nm NPs, the diffusion rate and cellular uptake kinetics of 50 nm NPs result in an extended residence time within tumor tissue.

DOI: 10.54254/2753-8818/2026.AU29754

3.2. Effect of nanomedicine structure and shape on therapeutic efficacy

Nanomedicines have specific structural and morphological requirements. Reports indicate that, due to shape-induced differences in surface area, human cells exhibit varying degrees of uptake efficiency for nanomedicines of different shapes; additionally, the drug-loading capacity of nanomedicines varies with their structural design.

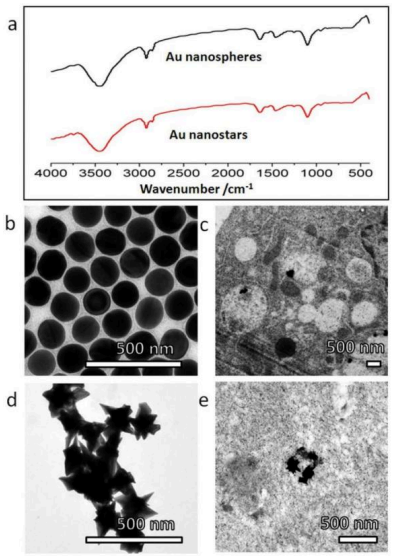


Figure 2. The differences in cellular behavior between gold (Au) nanospheres (low sharpness) and Au nanostars (high sharpness) were observed via transmission electron microscopy (TEM). (a) Identical features in the Fourier transform infrared spectroscopy (FTIR) spectra of Au nanospheres and Au nanostars confirm their similar surface chemistry. (b) TEM image of Au nanospheres. (c) Typical TEM images showing the stable localization of Au nanospheres within membrane-bound vesicles in cells following 24 hours of incubation in serum-free medium. (d) TEM image of Au nanostars. (e) Typical TEM images showing the distribution of Au nanostars in the cytoplasm of cells following 24 hours of incubation in serum-free medium

Figure 2 shows the surfaces of Au nanostructures were modified with polyethylene glycol (PEG), resulting in a methoxy-dominant surface chemistry. Two types of Au nanostructures were selected: spherical Au nanospheres with a diameter of 150 nm and spiky Au nanostars with a size of 150 nm [12]. Following 24 hours of incubation of HepG2 cells with the two respective Au NPs, approximately 90% of the Au nanoparticles were localized within membrane-bound vesicles, whereas ~95% of the Au nanoparticles were found in the cytoplasm. These experiments revealed that Au nanospheres were easily excreted by cells, whereas Au nanostars were retained more effectively (i.e., cellular excretion was more difficult).

This study analyzes drug release rates, whereas pharmacokinetics focuses on the relationship between drug release and time. Kinetic data enable the investigation of various influencing factors. This study classifies the mechanisms of controlled drug release into five categories: (1) diffusion-controlled, (2) degradation- and dissolution-controlled, (3) solvent-activated, (4) ion-exchange-controlled, and (5) magnetic-controlled. In diffusion-controlled systems, drugs are released via diffusion through polymers. In degradation- and dissolution-controlled systems, drugs are released as a result of polymer degradation or the gradual dissolution of the entire carrier. For most controlled drug release systems, diffusion-controlled and degradation-dissolution-controlled mechanisms

DOI: 10.54254/2753-8818/2026.AU29754

operate synergistically. Current research on the integration of polymeric materials (as carriers) with drugs primarily involves three forms: drug encapsulation, homogeneous mixing, and polymer-drug conjugates [13]. These three forms exhibit distinct drug release mechanisms. Encapsulation-based controlled drug release systems physically embed drugs within polymer membranes, enabling drug release via diffusion through the membrane. Homogeneous mixing-based controlled drug release systems involve the uniform dispersion of drugs within a polymer matrix, with drug release occurring via diffusion coupled with the synergistic degradation and dissolution of the polymer [14]. Polymer-drug conjugates refer to drugs covalently linked to polymers, with drug release triggered by chemical bond cleavage reactions.

4. Calculation of the appropriate size of nanomedicines

4.1. Parameters in the Higuchi model

Owing to the Higuchi model's excellent ability to describe diffusion-dominated release systems and its good compatibility with other models, this study primarily employs the Higuchi model for simulations.

For the simplified analysis of the Higuchi model, the value of k was first hypothesized, followed by simulations of spherical polymeric nanodrugs. The spherical coordinate diffusion equation was introduced, and the parameter relationship of k was adjusted:

$$k = A\sqrt{\frac{DC_s\varepsilon}{\tau \bullet f(r)}} \tag{1}$$

It can be observed that k is associated with D (diffusion coefficient), C_s (solubility), ε (porosity), τ (tortuosity factor), and $f(r)$ (size correction factor for spherical particles).

Subsequently, relevant parameters were determined by integrating the bone microenvironment and spherical nanoparticles: the dense bone matrix and collagen fibers may increase the tortuosity of the diffusion path, while enzymes (e.g., matrix metalloproteinases) or an acidic environment may accelerate carrier degradation. The dynamically changing leaky characteristics of bone tumor blood vessels enable the passive targeting of 30–200 nm particles, although the dense stroma restricts deep penetration.

It can be inferred that the diffusion coefficient D is influenced by the viscosity of the bone matrix and nanoparticle size:

$$D \propto \frac{T}{\eta r} \tag{2}$$

$$D = \frac{k_B T}{6\pi\eta r} \tag{3}$$

The initial value of porosity ε is determined by the nano particle material, and it can be calculated due to the increasing characteristics of nano medicine after degradation,

$$\varepsilon(t) = \varepsilon_0 + \alpha t \tag{4}$$

In the bone microenvironment, $\alpha \approx 0.01 h^{-1}$, $\varepsilon_0 \approx 0.2$..

The tortuosity factor τ increases the complexity of the diffusion path due to the dense collagen network of the bone matrix, with $\tau \approx 3-5$.

DOI: 10.54254/2753-8818/2026.AU29754

The size correction factor $f(r)$ accounts for the influence of the surface area-to-volume ratio of spherical particles on diffusion efficiency:

$$f(r) \propto r^{-1} \tag{5}$$

$$f(r) = 1 + \beta/r \tag{6}$$

For polymeric nanoparticles, $\beta \approx 5 - 20\text{nm}$.

Parameter A represents the total drug concentration per unit volume of the matrix. M is the drug mass, and V is the total volume of the nanoparticle; \ (A \) is calculated using the following formula:

$$A = \frac{M}{V}, A \gg C_s \tag{7}$$

Here, C_s represents the maximum solubility of the drug in the release medium and is influenced by interactions between drug molecules and the medium.

According to the Ostwald–Freundlich equation, the solubility of nanoparticles $C_s^{\text{nanometre}}$ increases as particle size decreases:

$$ln(\frac{C_s^{nanometre}}{C_s^{bulk-phase}}) = \frac{2\gamma V_m}{rRT} \tag{8}$$

Incorporating the above formulas into the derivation of \ (k \), the following expressions are obtained:

$$K = A\sqrt{\frac{C_s \bullet (\frac{k_B T}{6\pi\eta r}) \bullet (\varepsilon_0 + \alpha t)}{\tau \bullet (1+\beta/r)}} \tag{9}$$

$$k \propto A\sqrt{\frac{TC_s}{\eta\tau r^2} \bullet \frac{\varepsilon_0 + \alpha t}{1+\beta/r}} \tag{10}$$

4.2. Simulation of nanomedicine diffusion

Based on the above constraints, the following assumptions were made: $T = 310\text{K}, \eta = 1.2\text{mPa} \bullet \text{s}, \varepsilon_0 = 0.2, \tau = 4$.

Owing to the limitations of the EPR effect, nanoparticles were initially assumed to have sizes ranging from 30 to 200 nm, corresponding to a k value range of $2.0 - 12.5\mu\text{g} \bullet \text{mm}^{-2} \bullet \text{h}^{-\frac{1}{2}}$.

Integrating the properties of polymeric nanodrugs and the bone microenvironment, the Higuchi model was used to simulate the drug release rates of polymeric nanodrugs. First, simulations were performed under a simplified model, $k = 10.0\mu\text{g} \bullet \text{mm}^{-2} \bullet \text{h}^{-\frac{1}{2}}$, as can be observed in Figure 3. Simulated drug release rates over time:

DOI: 10.54254/2753-8818/2026.AU29754

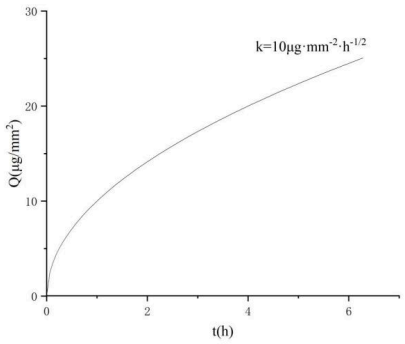


Figure 3. Drug release profiles under the simplified model, demonstrating a gradual decrease in drug release rate over time

However, Koizumi, Panosuk, and colleagues applied the drug release model to spherical Higuchi carrier devices with dissolved polymers as substrates. Additionally, Siepmann et al. validated the drug release model using PLGA spherical drug carriers loaded with 5-fluorouracil and observed a high degree of compliance [15].

The Bank–Lonsdale model, which describes drug release from spherical matrices, is expressed as [16]:

$$f_1 = \frac{3}{2}\left[1-\left(1-\frac{M_t}{M\infty}\right)^{\frac{2}{3}}\right]-\frac{M_t}{M\infty} = k_{BL}t \tag{11}$$

$\mathrm{M_t}$: The proportion of total drug released at time t (The scope is $0\text{~}100\%$).

$\mathrm{M_\infty}$: The total amount of drug released after an infinite amount of time (i.e., the total drug load).

$\mathrm{k_{BL}}$: Baker-Lonsdale release rate constant (the inverse of the time dimension, such as $\mathrm{h^{-1}}$).

The Bank–Lonsdale model was then used to simulate drug release from spherical matrices. First, in an ideal model, $\mathrm{M_\infty = 100\%}$, $\mathrm{K_{BL} = 0.05h^{-1}}$ were assumed.

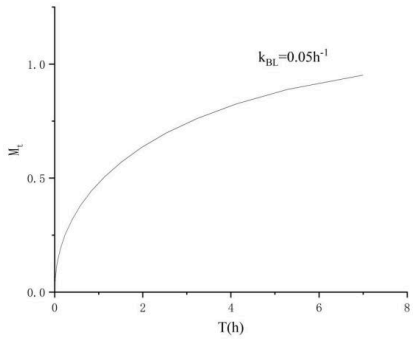


Figure 4. Simulation of the Bank–Lonsdale model with$\mathrm{K_{BL} = 0.05h^{-1}}$

It can be observed that the drug release rate also decreases with increasing time; however, compared with the general Higuchi model, the change in drug release rate during the initial period is relatively small (like Figure 4).

DOI: 10.54254/2753-8818/2026.AU29754

Subsequently, different k values were assigned to simulate drug release rates under varying k conditions:

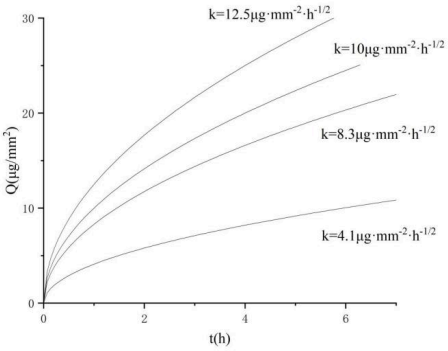


Figure 5. Simulation of the Higuchi model with different k values

Figure 5 shows that can be observed that the drug release rate increases with increasing k values. Conversely, lower k values result in reduced release rates and make it difficult to achieve sufficient drug release.

4.3. Analysis of nanodrug size range

Table 1. Assume that r=30,80,150nm is put into the model to calculate k value

r(nm)	k($\mu g \cdot mm^{-2} \cdot h^{-1/2}$)
30	12.5
80	8.3
150	4.1

Integrating data in the table 1, the following conclusions can be drawn:

$r < 50nm$: Nanoparticles exhibit a high diffusion rate; however, their small size leads to rapid clearance by organs such as the kidneys, preventing efficient drug uptake by cancer cells.

$50nm < r < 150nm$: The EPR effect is significant, and $k \propto r^{-1}$.

$r > 150nm$: Nanoparticles exhibit poor permeability and may result in incomplete drug release.

4.4. Calculation of the optimal nanomedicine size range

Subsequently, the optimal size range for nanomedicine fabrication was calculated. First, the EPR effect efficiency function—targeting efficiency $E(r)$ —can be approximated by a Gaussian distribution:

$$E(r) = e^{-\frac{(r-200)^2}{2\times 30^2}} \tag{12}$$

The peak of this distribution occurs at $r = 100nm$.

Tissue penetration depth, denoted as $p(r)$, is negatively correlated with nanoparticle size:

$$P(r) = \frac{500}{1+(\frac{r}{80})^2}\,\mu m \tag{13}$$

DOI: 10.54254/2753-8818/2026.AU29754

When $\mathrm{r}=80\mathrm{nm}$, $\mathrm{P}_{80}=250\mu\mathrm{m}$

Given that the renal clearance threshold is <10nm and the splenic clearance threshold is > 150nm, the retention time $\mathrm{T}(\mathrm{r})$ can be approximated as:

$$T(r)=\frac{48}{1+e^{-\frac{r-60}{20}}}\,h \tag{14}$$

Considering the toxicity of nano medicine, assume that $\mathrm{Toxicity}\left(\mathrm{r}\right)\propto\frac{1}{\mathrm{T}(\mathrm{r})}$,

Thus, the evaluation function $\mathrm{Assess}(\mathrm{r})$ can be designed

$$\mathrm{Assess}(\mathrm{r})=\mathrm{k}\times\mathrm{E}(\mathrm{r})\times\mathrm{P}(\mathrm{r})\times\mathrm{T}(\mathrm{r})^{2} \tag{15}$$

When $\mathrm{r}=80\mathrm{nm}$, The evaluation effect is optimal

Take the range above 95%, and the design works good at 80-120nm .

5. Conclusion

The therapeutic efficacy of nanodrugs for bone cancer is influenced by multiple factors. To achieve favorable therapeutic outcomes, this study focused on optimizing nanoparticle size. Building on the size dependence of nanomedicines in the bone microenvironment, the optimal size of nanomedicines for this microenvironment was systematically investigated and calculated. Through various simulation experiments and data analysis, the interactive relationships between nanodrug size and various physiological factors in the bone microenvironment were thoroughly analyzed. The results demonstrate a non-monotonic relationship between nanoparticle size (20–300 nm) and bone targeting efficiency: ultrafine particles (< 50 nm) exhibit a high diffusion coefficient but are rapidly cleared by bone marrow sinuses, while larger particles (> 150 nm) are restricted by the narrow channels of the lacunar-canalicular network (LCN) within osteons.

Although this study successfully identified the optimal size range of nanomedicines for the bone microenvironment, it has certain limitations. Future studies should further consider the dynamic changes in the bone microenvironment and the impact of nanodrug surface properties on their behavior to more accurately optimize nanomedicine design. For instance, investigating the influence of osteoclast activity on nanomedicine distribution could provide more rational theoretical guidance for the design of spherical polymeric nanodrugs and offer more effective strategies for the treatment of bone diseases.

References

[1] Vlenterie, M., Litière, S., Rizzo, E., Marréaud, S., Judson, I., Gelderblom, H., Le Cesne, A., Wardelmann, E., Messiou, C., Gronchi, A., & van der Graaf, W. T. (2016). Outcome of chemotherapy in advanced synovial sarcoma patients: Review of 15 clinical trials from the European Organisation for Research and Treatment of Cancer Soft Tissue and Bone Sarcoma Group; setting a new landmark for studies in this entity. European journal of cancer, 58, 62–72.

[2] D'Oronzo, S., Coleman, R., Brown, J., & Silvestris, F. (2018). Metastatic bone disease: Pathogenesis and therapeutic options: Up-date on bone metastasis management. Journal of bone oncology, 15, 004–4.

[3] Włodarczyk, R., & Kwarciak-Kozłowska, A. (2021). Nanoparticles from the Cosmetics and Medical Industries in Legal and Environmental Aspects. Sustainability, 13(11), 5805.

DOI: 10.54254/2753-8818/2026.AU29754

[4] Akanda, M., Mithu, M. S., & Douroumis, D. (2023). Solid lipid nanoparticles: An effective lipid-based technology for cancer treatment. Journal of Drug Delivery Science and Technology, 86, 104709
[5] Fritton, S. P., & Weinbaum, S. (2009). Fluid and Solute Transport in Bone: Flow-Induced Mechanotransduction. Annual review of fluid mechanics, 41, 347–374.
[6] Lin-Ping Wu, Danyang Wang, Zibiao Li, Grand challenges in nanomedicine, Materials Science and Engineering: C, Volume 106, 2020, 110302, ISSN 0928-4931.
[7] Jakonyte, A., Gustainyte, E., Petronis, Z., Hafizov, A., Janovskiene, A., & Razukevicius, D. (2025). Risk of Osteonecrosis of the Jaw in Patients Treated with Zoledronic or Alendronic Acid: A Systematic Review. Medicina (Kaunas, Lithuania), 61(7), 1159.
[8] Chiang, C.-L.; Cheng, M.-H.; Lin, C.-H. From Nanoparticles to Cancer Nanomedicine: Old Problems with New Solutions. Nanomaterials 2021, 11, 1727. https: //doi.org/10.3390/nano11071727
[9] Jérôme, C., & Lecomte, P. (2008). Recent advances in the synthesis of aliphatic polyesters by ring-opening polymerization. Advanced drug delivery reviews, 60(9), 1056–1076.
[10] Tang, L., Yang, X., Yin, Q., Cai, K., Wang, H., Chaudhury, I., Yao, C., Zhou, Q., Kwon, M., Hartman, J., Dobrucki, I., Dobrucki, L., Borst, L., Lezmi, S., Helferich, W., Ferguson, A., Fan, T., & Cheng, J. (2014). Investigating the optimal size of anticancer nanomedicine. Proceedings of the National Academy of Sciences of the United States of America, 111(43), 15344–15349.
[11] Tchoryk, A., Taresco, V., Argent, R. H., Ashford, M., Gellert, P. R., Stolnik, S., Grabowska, A., & Garnett, M. C. (2019). Penetration and Uptake of Nanoparticles in 3D Tumor Spheroids. Bioconjugate chemistry, 30(5), 1371–1384.
[12] Chu, Z., Zhang, S., Zhang, B., Zhang, C., Fang, C.-Y., Rehor, I., Cigler, P., Chang, H.-C., Lin, G., Liu, R., & Li, Q. (2014). Unambiguous observation of shape effects on cellular fate of nanoparticles. Scientific Reports, 4, 4495.
[13] Gupta, N., & Saha, S. (2025). Polymer-Based Designer Particles as Drug Carriers: Strategies to Construct and Modify. ACS applied bio materials, 8(6), 4432–4466.
[14] Pillai, A., Bhande, D., Pardhi, V. (2023). Controlled Drug Delivery System. In: Santra, T.S., Shinde, A.U.S. (eds) Advanced Drug Delivery. Studies in Mechanobiology, Tissue Engineering and Biomaterials, vol 26. Springer, Singapore.pp 267–289.
[15] Faisant, N., Siepmann, J., & Benoit, J. P. (2002). PLGA-based microparticles: elucidation of mechanisms and a new, simple mathematical model quantifying drug release. European journal of pharmaceutical sciences : official journal of the European Federation for Pharmaceutical Sciences, 15(4), 355–366.
[16] Paarakh, M., Jose, P., Setty, C., & Christoper, G., (2019). Release kinetics – concepts and applications. International Journal of Pharmacy Research & Technology.